Eur. Phys. J. B **7**, 37–51 (1999)

THE EUROPEAN PHYSICAL JOURNAL B

EDP Sciences

Spectral properties of the attractive Hubbard model

J.M. Singer[a], T. Schneider, and P.F. Meier

Physikinstitut, Universität Zürich, Winterthurerstrasse 190, 8057 Zürich, Switzerland

Received: 7 July 1998 / Accepted: 30 July 1998

Abstract. We calculate the spectral functions, the band structure and the density of states of the 2D attractive Hubbard model in the intermediate coupling regime (*i.e.* the crossover regime between BCS theory and Bose-Einstein Condensation) using a grand canonical quantum Monte-Carlo approach and a maximum entropy procedure. The evolution of the spectral properties as a function of temperature is discussed. In particular, on lowering the temperature, we find a splitting of the single band present at high temperatures into several distinct branches, the number of which depends on the temperature.

PACS. 74.20.-z Theories and models of superconducting state – 74.25.Dw Superconductivity phase diagrams – 71.10.Fd Lattice Fermion models (Hubbard model, etc.)

1 Introduction

The problem of a crossover from a weak coupling BCS (Bardeen-Cooper-Schrieffer, [1]) picture of Cooper pair formation and condensation at a critical temperature to a Bose-Einstein condensation (BEC, [2]) of preformed (local) pairs has recently attracted great attention. The motivation to study this problem comes from experimental observations regarding unusual properties of the high-T_c cuprate superconductors. Particularly interesting in this respect are recent experiments showing a pseudo-gap structure in the normal-state density of states of underdoped cuprates that persists almost up to room temperature [3–7]. A further unusual property different from conventional BCS-type superconductors is the extreme short coherence length (of the order of some lattice constants) of the pairs in the superconducting state, much smaller than in usual superconductors (where it is of the order of several thousand Å).

To gain insight into the electronic properties of the normal and superconducting states we explore the effect of electron correlations, and in particular pair formation and appearance of superconducting correlations, on the density of states, the spectral densities and the band structure in a rather simplified lattice model system, the two-dimensional Hubbard model with local attractive interaction (2AHM). Although this model is unlikely to provide a microscopic description of high-temperature superconductivity, it serves rather well to reveal the effect of correlations on measurable properties. It is evident that the local attractive onsite density-density interaction term favors double occupancy of sites and hence the formation of (s-symmetric) pairs. If these pairs of charge $2e$ are mobile, superconductivity will occur below a certain temperature.

[a] e-mail: jms@physik.unizh.ch

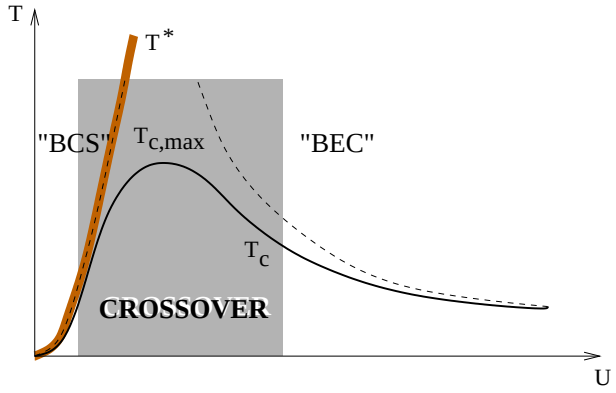

Fig. 1. "Sketch" of the crossover regime along the coupling strength axis U for fixed density ρ. Shown are qualitative curves for the critical temperature T_c, as obtained *e.g.* by QMC (solid line), as well as the BCS and BEC limits (dashed lines). Additionally, a T^* curve is drawn (dark gray curve), indicating the pair formation scale in contrast to the condensation temperature T_c.

This model exhibits a pronounced crossover (see illustration in Fig. 1) from a weak coupling regime, where the essential features of the superconducting state are well described by a BCS theory, to a strong coupling regime, properly described by a BE condensation of local, preformed (real-space) pairs. Because of its conceptual simplicity, the attractive Hubbard model allows an easy investigation of the crossover from weak to strong coupling, from extended to local pairs, from BCS to BEC, just by tuning the interaction parameter U (Fig. 1), which acts as a control parameter for the phase transition line in analogy to the carrier doping in *e.g.* the high temperature superconducting cuprates. At sufficiently low T an instability

of the Fermi sea towards superconductivity occurs, the transition is essentially mean-field in character, see *e.g.* [8–10] and references therein. This link of the weak coupling regime with BCS superconductivity has been provided by Schmitt-Rink and Nozières [11]. The evolution from Cooper-pair superconductivity for small U to local pair superconductivity for large U is smooth.

In the present work the electronic carrier density ρ ("electron doping", charge carriers per site and spin) is assumed to be finite and fixed, away from half-filling. In Figure 1 we sketch a qualitative T-U-phase diagram, as discussed *e.g.* in [10], and indicate the $T_c(U)$ curve as obtained by QMC together with the BCS and BEC limits. Moreover, we plot in this figure also a T^*-curve, giving the pair formation energy scale. Since at both endpoints of this phase transition line, the $U = 0$ and the $U \to \infty$ limit, T_c vanishes, it is evident that there must be an optimal T_c for an intermediate value of U [10]. For $U = 0$ we have a normal metal. For $U \to \infty$ the electrons form bound pairs which are immobile since they can only move *via* virtual ionization with an infinite energy barrier. On the lattice, T_c vanishes in this limit, while in the continuum limit it remains finite [12,13]. This difference is due to the absence of a pair hopping term when working on a lattice. For increasing coupling strength T_c is suppressed by fluctuations down from the BCS value T_c^{BCS}, and T_c^{BCS} becomes rather a mere pair formation scale. T_c^{BCS} is no longer connected to the condensation temperature, where long range order is established.

A large number of studies has been published discussing several aspects of this crossover. Here we will provide an extension of the earlier work, we put special emphasis on the discussion of the spectral properties and their temperature evolution in the intermediate coupling regime, which is particularly difficult to access by any kind of approximative method. In the intermediate coupling regime the physics will be dominated by the interplay between quasiparticles and bound pairs, leading to nontrivial behavior. We therefore concentrate on the investigation of the attractive Hubbard model with the quantum Monte-Carlo (QMC) approach, which has the potential to treat this type of strongly correlated system on a lattice numerically exactly, allowing us to go far beyond certain approximative methods.

2 The attractive Hubbard model

We consider the 2D attractive Hubbard model (2AHM, "negative-U model") on a square lattice:

$$\mathcal{H} = -t \sum_{\langle ij \rangle \sigma} (c_{i\sigma}^\dagger c_{j\sigma} + h.c.) - U \sum_i n_{i\uparrow} n_{i\downarrow} - \mu \sum_{i\sigma} n_{i\sigma}, \tag{1}$$

where $c_{i\sigma}^\dagger$ ($c_{i\sigma}$) denote fermionic creation (annihilation) operators at site i with spin σ, and t is the kinetic term between two neighboring sites, which serves as an energy unit throughout the paper. The limit $\langle ij \rangle$ restricts the sum to next-neighbors, U denotes the interaction ("coupling"), which is chosen to be attractive, and μ is the chemical potential. We consider the intermediate coupling regime $W/2 \leq U \leq W$, W being the bandwidth ($W = 8t$ in $D = 2$). Away from half-filling the 2AHM is believed to undergo a Kosterlitz-Thouless (KT) [14] transition.

In the free case ($U/t = 0$) we have the well-known dispersion relation for the D-dimensional system,

$$\epsilon(k) = -2t \sum_{\alpha=1}^{D} \cos(k_\alpha) - \mu. \tag{2}$$

With the exception of the critical endpoints and $\rho = 0.5$ (ρ is the density of electrons per site and per spin, *i.e.* $\rho = 1$ corresponds to the fully occupied lattice with 2 electrons of opposite spin at each site), the phase transition line is supposed to be a line of D-dimensional XY critical points, while the special point $\rho = 0.5$ corresponds to a D-dimensional XYZ critical point. For this reason, the transition temperature vanishes in 2D at $\rho = 0.5$ (half-filling). There one finds a coexistence of superconducting and long-range charge-density correlations, which, in 2D, drive the effective KT transition temperature to zero ($T_{KT}^{2D}(\rho = 0.5) = 0$), accounting for another critical point $\rho_{c,2D} = 0.5$. At zero temperature, $T = 0$, there are two critical endpoints, namely $\rho_c = 0$ and $\rho_c = 1$, where the model undergoes an insulator to superconductor transition.

In a strictly two-dimensional superconductor, thermal fluctuations will destroy "true" long-range order for all $T > 0$, but a KT transition may still separate two phases. The low temperature phase is characterized by a finite superfluid density and correlations that decay algebraically with distance. In a finite, periodic lattice, the correlations might well level off similar to a "conventional" phase transition, thus enabling us to study effects of a "quasi-conventional" transition even in 2D, with a size-dependent critical temperature. A proper scaling leads in fact to the "real" KT temperature [15]. We will make use of this (in a strict sense) "size" effect when we study the temperature evolution of the spectral properties of a 2D system.

In addition to the density-driven transitions at fixed U there are also interaction driven transitions at fixed ρ. These have been discussed earlier on from a phase transition point of view [10]: as a function of coupling strength U and fixed ρ there is a phase transition line with critical endpoints $U = 0$ and $U \to \infty$. At $T = 0$ a normal metal to superconductor transition occurs at $U = 0$, while for $U \to \infty$ there is a superconductor-localization (insulator) transition. In the strong coupling regime this model can be mapped onto hard core bosons on a lattice, in which Cooper pairs are treated as conserved particles obeying Bose statistics.

The nature of the phase transition is quite different in the two limits: in the weak coupling, BCS-like limit a formation of Cooper pairs and their condensation takes place simultaneously at T_c. A first deviation from this scenario is usually described in terms of superconducting fluctuations. In the preformed pair (BEC) regime, however,

the pair formation at T^* and their condensation at T_c are independent processes. T^* and T_c are widely separated, with T^* being only a characteristic energy scale, not a phase transition temperature. For $T > T^*$ the pairs are thermally dissociated. In the weak coupling limit, below T_c, we have a BCS-type condensate of strongly overlapping Cooper pairs. Thermodynamics and T_c are determined by single particle excitations (broken Cooper pairs, quasi-particles). In the opposite, strong coupling regime one has a Bose condensate of tightly bound local pairs, and thermodynamics and T_c are governed by the collective modes. For a review see *e.g.* [16], the crossover has been studied by a series of authors [2,8–11,16–25].

3 Technique

We present numerical studies of the described model using a particular type of quantum Monte-Carlo (QMC) method, the temperature dependent QMC formulation in the grand canonical ensemble (after Hirsch *et al.* [26–29]). We emphasize that the QMC approach has the potential to treat these types of strongly correlated systems, allowing us to go far beyond certain approximative methods. It provides an approximation-free, numerically exact ansatz (besides controllable statistical errors), unlike most standard analytical techniques, and yields information about systems much larger than those accessible by exact diagonalization algorithms. The QMC method uses the Suzuki-Trotter and the Hubbard-Stratonovich transformation to "break up" the quantum-mechanical many-particle system. Applying these methods to the attractive Hubbard model frees us from the central drawback of fermion QMC calculations, the so-called "sign problem". This allows us to perform reliable and stable calculations over a vast parameter range

To extract spectral properties of the Hubbard model we retrieve time-dependent correlation (Green's) functions (in imaginary time), which may be written

$$G_\sigma(i-j,\tau) = -\langle T_\tau c_{i\sigma}(\tau) c^\dagger_{j\sigma}(0)\rangle \ . \tag{3}$$

As we are merely interested in dynamical properties at finite temperatures, we restrict ourselves to the evaluation of this quantity in the grand canonical algorithm; a scheme for the application in the $T = 0$-formalism projector QMC was introduced by von der Linden [30] and applied in [27]. The analytic continuation seeks to extract real frequency, dynamical information from these imaginary-time correlation functions computed in QMC simulations. The imaginary-time Green's functions $G(k,\tau)$ in k-space are intimately connected to the spectral function $A(k,\omega)$ *via*

$$G(k,\tau) = \begin{cases} -\displaystyle\int_{-\infty}^{\infty} d\omega \frac{\exp(-\omega\tau)}{\exp(-\beta\omega)+1} A(k,\omega) \text{ if } \tau > 0 \\ +\displaystyle\int_{-\infty}^{\infty} d\omega \frac{\exp(-\omega\tau)}{\exp(+\beta\omega)+1} A(k,\omega) \text{ if } \tau < 0 \end{cases} \tag{4}$$

from which we can easily obtain the density of states as a summation over all k-states:

$$N(\omega) = \frac{1}{N}\sum_k A(k,\omega). \tag{5}$$

We seek these spectral densities because linear-response theory relates these functions to experimentally measurable quantities.

But, these simple equations pose a serious problem: the correlation functions are easy to obtain, but it is rather difficult to extract the spectral properties from the computed QMC data because an analytic continuation, or rather an inverse Laplace transformation from imaginary to real time, is required. This inversion of QMC data (and usually of all statistically computed data) is extremely numerically illposed due to two obvious reasons: data are available only for a limited set of imaginary times and the data are usually more or less noisy. As a consequence, the solution might not be unique in general.

The method of choice is the maximum entropy (MaxEnt) ansatz, as proposed by Gubernatis, Jarrell and coworkers [31,32] for a similar type of data. The method we used to obtain the presented information is a slight variation of this ansatz after von der Linden's work [30]. The MaxEnt technique approaches statistical data analysis within the concepts of conditional probabilities (Bayesian logic), where the spectral density is regarded as a probability function, and what is extracted from the data is the most probable spectral density [31]. Unique about the MaxEnt approach is the specification of the prior probability function of the solution in terms of the information-theory definition of entropy.

4 Results

In the following section we will discuss our results for the density of states $N(\omega)$, the k-resolved spectral density $A(k,\omega)$ and the band structure $\Omega(k,\omega)$. We concentrate on three different parameter sets in the intermediate coupling (crossover) regime:

1. $U/t = 4$, $\rho = 0.25$ ("quarter-filling") at $N = 16 \times 16$,
2. $U/t = 6$, $\rho = 0.4$ (close to half-filling) at $N = 16 \times 16$,
3. $U/t = 8$, $\rho = 0.1$ (low-density limit) at $N = 10 \times 10$.

Additionally, to allow a comparison along the U / fixed ρ-axis, we provide some data for two further parameter sets at only one fixed temperature value $T/t = 0.5$: $U/t = 4.0$, $\rho = 0.4$ and $U/t = 8.0$, $\rho = 0.4$.

These systems have been chosen, since they allow us to present a wide overview on the behavior in the intermediate regime. Simultaneously, we can use our computational resources in the most economical way. The system size 16×16[1] represents the uppermost system size giving reasonable computer times for this type of simulation (we use single nodes of an IBM SP2 system), *i.e.* giving us still the chance to produce excellent statistics

[1] Periodic boundary conditions are applied.

(*i.e.* long enough runs to reduce statistical noise). For the low-density ($U/t = 8$, $\rho = 0.1$) run we even lowered the size in favor of an enlarged number of independent MC bins and prolonged Markov chains, and thus even smaller statistical errors. The reason is that for $\rho \to 0$ the MaxEnt procedure becomes unusually difficult, whereas for larger U the statistical fluctuations along the MC time axis increase and thus we need longer runs to produce statistical error bars comparable to the lower U simulations. Of particular interest is certainly the regime in parameter space close to half-filling, since there almost all techniques besides QMC/MaxEnt fail to produce reasonable results. The critical temperatures of the three systems are approximately in the same range[2], for example, $T_c/t(U/t = 4.0, \rho = 0.25) \simeq 0.11$. A KT scaling analysis of the QMC data similar to the one proposed by Moreo *et al.* [15] yields for T_{KT} a slightly lower value, as confirmed by a recent analysis of enormously large lattices (128^2) using a T-matrix type of approximation [33]. On the other hand, we present for $U/t = 8.0$ data in the low density regime $\rho = 0.1$, since in this case we find at least some results from other methods [13,18,34]. It allows us to compare and interpret our findings. Using a phase diagram for this model, Figure 1, which has been presented in detail in an earlier publication [10], we would classify these parameters into three regimes:

- Regime 1, $U/t = 4.0$, lies on the BCS-side of the $T_c(U)$ curve, very close to the maximum;
- Regime 2, $U/t = 6.0$, lies on the BEC-side, very close to the maximum, and, thus, both 1 and 2 are deep inside the crossover regime. The T_c's of regime 1 and 2 are practically identical;
- Regime 3, $U/t = W = 8.0$ (with W being the bandwidth of the noninteracting system) is deeper inside the preformed-pair (BEC) regime, even given the fact, that the electronic filling is only $\rho = 0.1$.

We will discuss results for the density of states, then we will switch to the k-resolved spectral density, which will be subsequently used to draw a band structure. Finally we will plot k-space patches to discuss the evolution of the spectral properties in different regions of momentum space. Comparisons with results from other techniques, in particular BCS, will be given at the appropriate sections.

4.1 Density of states N(ω)

To start this section on QMC results for the density of states (DOS) we will present initially a non-QMC result: Figure 2 shows the density of states $N(\omega)$ for a "free", noninteracting system and a system with a finite coupling, treated in the simple BCS approach,

$$E^2(k) = \epsilon^2(k) + \Delta^2(k), \tag{6}$$

with Δ being an s-symmetric BCS gap function. The free system shows the usual 2D lattice system density of states,

[2] Technically, these temperatures can be reached by our stabilized QMC algorithm.

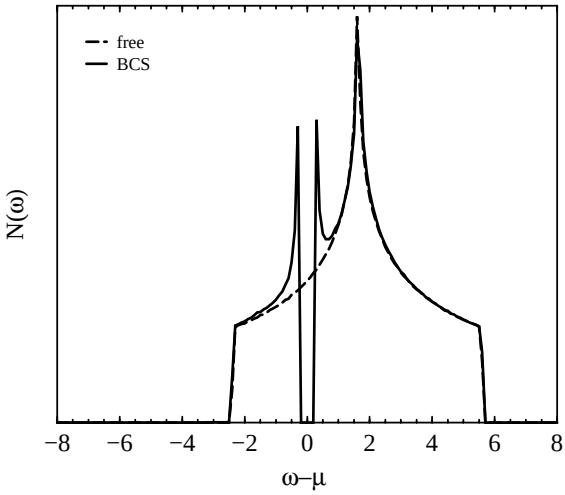

Fig. 2. Density of states $N(\omega)$ using $T = 0$ BCS-theory, electronic filling $\rho = 0.25$, free system, $U = 0$ (dashed line), and superconductor $U \neq 0$ (solid line). The calculation has been done on a lattice.

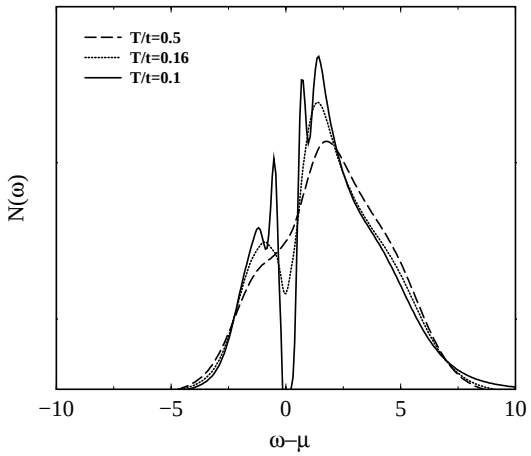

Fig. 3. Density of states $N(\omega)$, QMC, coupling strength $U/t = 4.0$, electronic filling $\rho = 0.25$, lattice size $N = 16 \times 16$, periodic boundary conditions.

with a van Hove singularity due to the characteristic saddle point. In contrast to the free system, the BCS result gives a gap structure around the chemical potential μ (*i.e.*, at $\omega - \mu = 0$), with the appearance of characteristic "coherence" peaks at the edge of the gap. These coherence peaks will be discussed in detail in a subsequent section. Despite of the usual thermal broadening for $T > 0$, these two curves characterize the DOS within the BCS mean-field approach. The appearance of a gap is intimately connected to the superconducting regime.

Figure 3 presents similar data obtained by QMC for three different temperatures (the band filling is chosen again to be $\rho = 0.25$). Here we find already a rather different behavior: for quite high temperatures (approx. $5T_c$) an initially small "deformation" of the DOS around the chemical potential begins to form, which, on lowering the temperature, develops into a "pseudo-gap" like

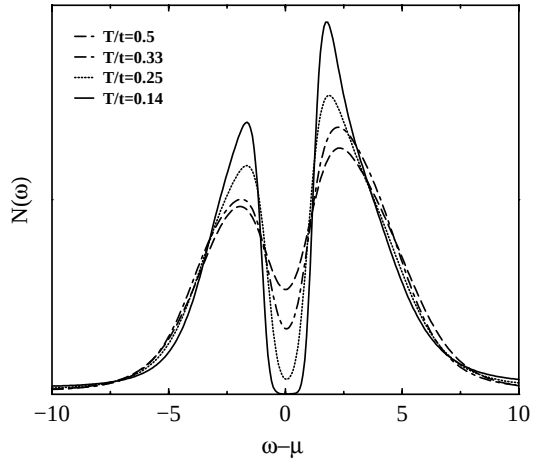

Fig. 4. Density of states $N(\omega)$, QMC, $U/t = 6.0$, $\rho = 0.4$, $N = 16 \times 16$.

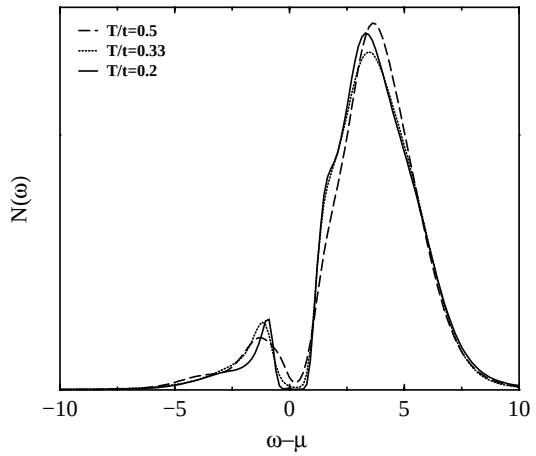

Fig. 5. Density of states $N(\omega)$, QMC, $U/t = 8.0$, $\rho = 0.1$, $N = 10 \times 10$.

dip. At $T/t = 0.1$ the system has reached the superconducting regime ($T_c/t = 0.11$), the gap is fully developed down to zero, and – characteristic for the superconducting state and similar to the BCS DOS – the typical peaks at the edge of the gap are present. Going to Figure 4 and thus increasing the coupling strength to $U/t = 6.0$ marks the onset of a crossover to a qualitatively different situation: a large pseudogap evolves already at high temperatures $T/t > 0.5$, but still the gap only "touches" zero and fully develops around the chemical potential close to $T_c/t \approx 0.14$, with the characteristic peaks at the edges of the gap starting to form. Due to the fact that the filling is close to halffilling it is hard to distinguish the peak located at positive frequencies from the remainder of the van Hove singularity, but there is a strong enhancement visible around T_c. Moreover, comparing Figure 5 with Figures 3 and 4 we see that the gap is already fully developed in the normal state far above T_c (see $T/t = 0.2$-curve, $T_c/t \approx 0.1$).

Additionally to the QMC- and BCS-DOS we include with Figure 6 a DOS for the 2AHM following the approach

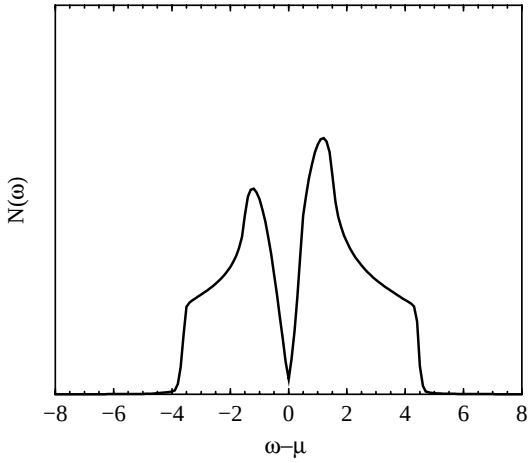

Fig. 6. Density of states $N(\omega)$, Schmid's ansatz [35] for the 2AHM, $\rho = 0.4$. The calculation uses a noninteracting density of states obtained for a discrete lattice.

introduced by Schmid [35] and later on reproduced and extended by Tchernyshyov [20] ([36] follows a similar argumentation). Their approach is of particular interest, since these authors studied the 2AHM assuming that superconducting long-range order is suppressed by strong 2D fluctuations. This is in fact true in a strict sense in the thermodynamic limit, as discussed earlier. In the regime below a BCS critical temperature, which now serves only as a pair formation scale, they find still a pseudo-gap (*i.e.* a suppression of the DOS at the chemical potential). But now the gap has a rather "unconventional" V-shaped form, normally attributed only to d-wave superconductors. Remind that the system under investigation is nevertheless still an s-wave superconductor. This pseudogap is only due to fluctuating pairs (Tchernyshyov [20] calls them "slow" fluctuations), and resembles the above-T_c pseudogap in Figure 3. Nevertheless, with increasing coupling strength U this picture becomes more and more inappropriate ($U/t \to \infty$ would cause an infinitely large fully developed gap at any temperature, with tightly bound pairs).

4.2 Spectral functions $\mathbf{A(k, \omega)}$

After describing results for the density of states $N(\omega)$, which is equal a k-summation over the spectral function $A(k, \omega)$, we will now focus on the k-resolved data. Sections 4.3 and 4.4 will discuss large k-space regions in detail. Initially we focus on two regimes of particular interest. These are the k-region which is formally associated with the Fermi surface k_F and secondly the k-region around the zone corners (π, π) and equivalent points. In fact, k_F is well defined only in the noninteracting and weak coupling regime, *e.g. via* the jump in $n(k)$ at k_F.

We would like to remark that the discussion of small finite lattices does not allow a decisive comment on Fermi-liquid *versus* no-Fermi-liquid behavior (*e.g.* on the basis of an analysis of the momentum distribution) in this intermediate regime. We will use the expression "Fermi edge"

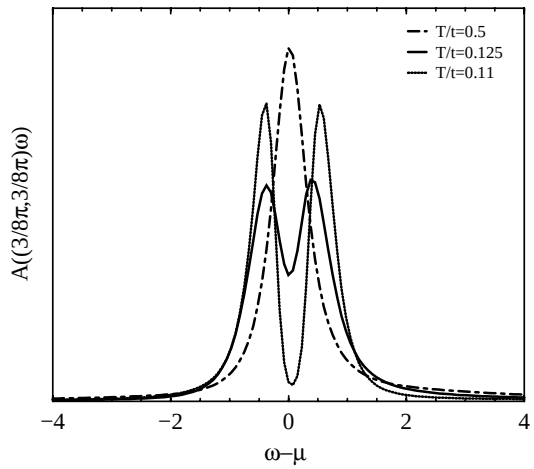

Fig. 7. Spectral function $A(k,\omega)$ for $k = (3\pi/8, 3\pi/8)$ and temperatures above T_c, $U/t = 4.0$, $\rho = 0.25$.

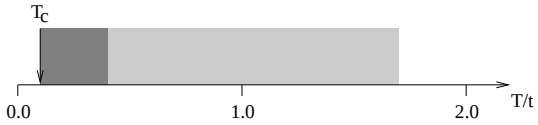

Fig. 8. "Temperature axis" for $U/t = 4.0$, $\rho = 0.25$: whereas $T_c \approx 0.11t$, the light shaded area marks the temperature window above T_c, where at least a second band is detectable ("pseudogap-regime"), and the narrow, dark shaded region gives the temperature, where the spectral function peak at the filling edge ("Fermi edge") starts to split ("fluctuation regime").

in the following text in a very loosely defined sense, which usually only indicates the "filling edge", *i.e.* $E - \mu = 0$.

Figure 7 presents data at k-points $(3\pi/8, 3\pi/8)$ and equivalent, which are as close as possible to the Fermi edge position of the non-interacting system for $\rho = 0.25$. There, for intermediate coupling $U/t = 4.0$ the system behaves qualitatively rather close to what we expect from the BCS theory, with some modifications around T_c. At high temperatures we find only one single peak, which is finally splitted by a gap around $\omega - \mu = 0$ below T_c. Here in our QMC results for the 2AHM this splitting initially starts in a rather small temperature window above T_c, which is probably defined to a large extent by thermal fluctuations. While at k_F there is only one single peak at *e.g.* $T/t = 0.5$, we would like to point to the fact that we have already two or more peaks in other k-regions (we will comment on that in Sects. 4.3 and 4.4). The splitting of the single peak at k_F into two maxima separated by a (superconducting) gap causes a shift of spectral weight away from $\omega - \mu = 0$ and, thus, a pile-up of two rather sharp "resonances" at the edge of the gap. This was already seen in the discussion of the density of states $N(\omega)$. The BCS theory would give an ungapped, single peak at the Fermi egde down to T_c, with a gap $\Delta(T)$ emerging only below T_c. An enhancement of the coupling strength, Figure 9 (due to the different value of ρ we have chosen another k-vector close to the assumed "Fermi" edge)

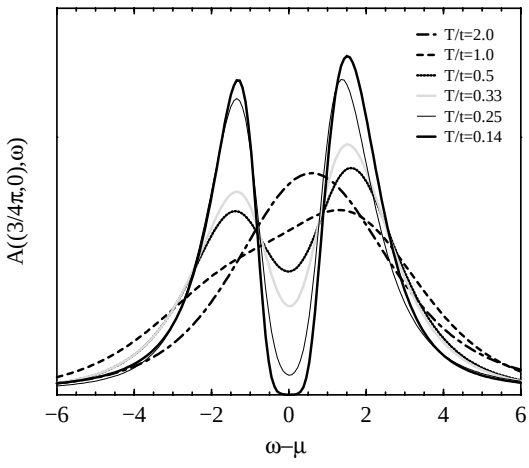

Fig. 9. Spectral function $A(k,\omega)$ for $k = (3\pi/4, 0)$ and temperatures above T_c, $U/t = 6.0$, $\rho = 0.4$.

shows, that there the splitting starts to form at much higher temperatures (in fact, almost an order of magnitude higher than for $U/t = 4.0$). The "fully" developed gap can still be found only at $T \approx T_c$. Again a pile-up of spectral weight at the gap edges can be detected. When we go to even larger U-values this picture changes qualitatively: the peak structure will be completely gapped at higher and higher temperatures far above T_c (see, *e.g.* the $U/t = 8.0$ band structure in Figs. 15 and 18), with the extreme limit of an infinitely wide gap at all temperatures for $U/t \to \infty$.

Furthermore, the region around the zone corners is of peculiar interest, in particular in the temperature window $T^* < T < T_c$. Figure 10 shows $A(k,\omega)$-data for the zone corner $k = (\pi, \pi)$ itself as well as for its closest neighbors along the (discrete) lattice axes and the diagonal. The data are obtained at $T/t = 0.5t$. In the left column of Figure 10 we keep the electron density fixed at $\rho = 0.4$ and increase the coupling strength from $U/t = 4$ to $U/t = 8$, going from top to bottom. The right column varies the density for the upper and lower row, thus enabling us to investigate the ρ-dependency of $A(k,\omega)$. The most striking feature is the appearance of not only two peaks, but three of them are visible, corresponding to at last three branches in the excitation spectrum. "At least" refers to the fact, that we are not able to reproduce the band structure itself, but only the positions of spectral peaks with a weight significantly different from zero. We would like to note that we cannot split "very close" lying peaks, in particular not if these peaks have a large difference in weight (*i.e.* a broad peak with large spectral weight will easily "cover" a small one in its tails).

The three peaks differ as follows: there is a large, broad peak (its position is marked Ω_1) at frequencies $\omega - \mu > 0$ (unoccupied range), a second broad one with low weight at the opposite side of the frequency axis (occupied range), marked Ω_2, and finally a third one, located close to the position of the chemical potential. Its position will be referred to as Ω_3, it is *e.g.* for $U/t = 6.0$, $\rho = 0.4$ located almost exactly at the chemical potential (*i.e.* $\Omega_3(\pi, \pi) = 0$).

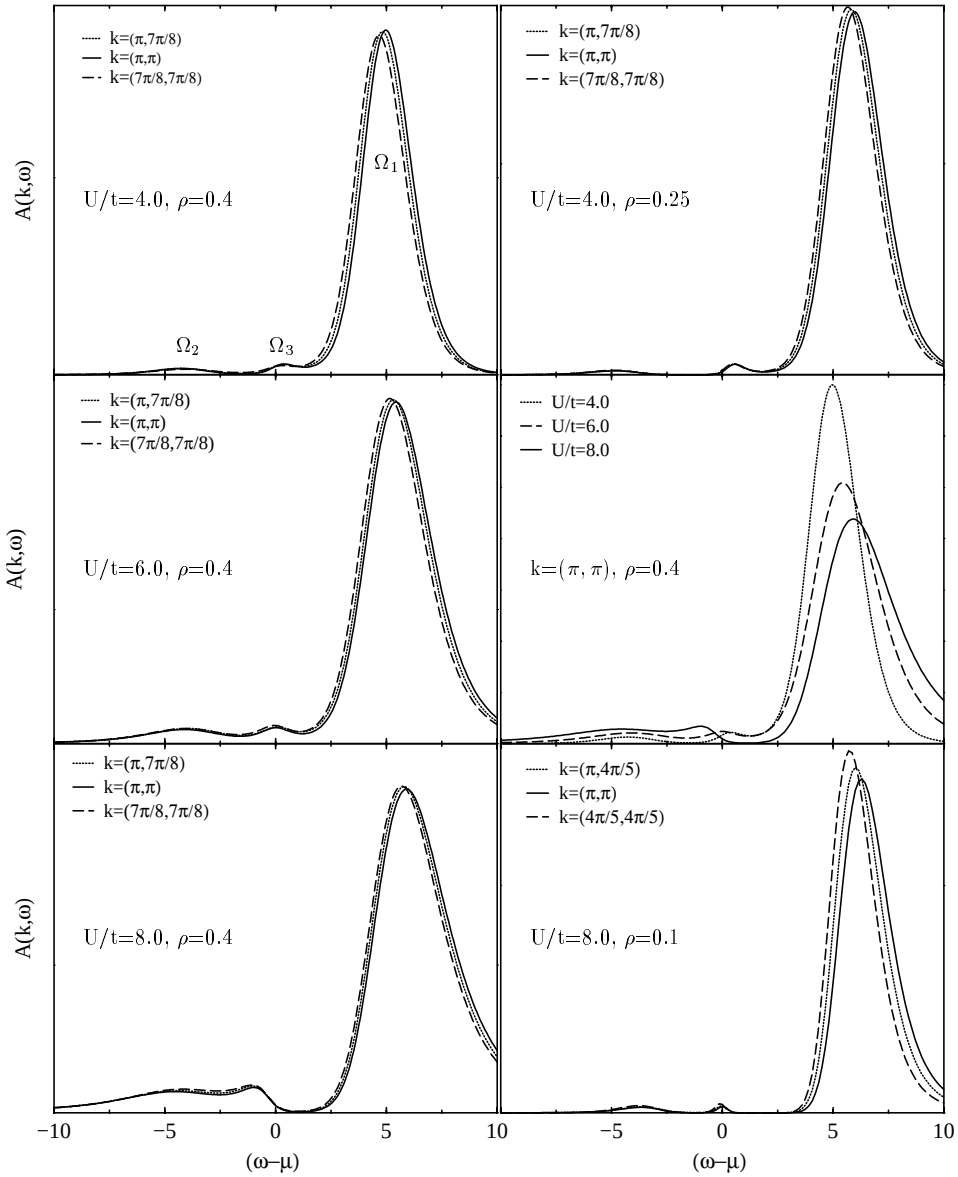

Fig. 10. Spectral function $A(k,\omega)$, k-vectors around (π,π), for $T/t = 0.5$ and different U-, ρ-values.

Ω_1, Ω_2 and Ω_3 shift as a function of doping as well as coupling (the coupling strength dependency is plotted in Fig. 11), but for all systems shown in Figure 10 there are clearly three peaks present. The spectral weight (relative to the Ω_1-peak) of the Ω_3-peak is lowest in the $\rho = 0.1$, $U/t = 8.0$ system, and largest in the $\rho = 0.4$, $U/t = 8.0$ system (there it accounts at its maximum for roughly 10% of the total spectral weight). The position of the Ω_3-peak shifts (a) to lower frequencies if the coupling strength U is increased and $\rho = const.$, and (b) to lower frequencies if the filling ρ is increased and $U = const.$ The spectral weight of Ω_3 increases with increasing coupling strength, and since both, the Ω_2- and Ω_3-line become broader and simultaneously seem to approach each other with increasing coupling strength (at least for $\rho = 0.4$), it will be increasingly difficult to split them from each other. The appearance of a third peak (band) around the zone corners in the normal state of the 2AHM is not totally unexpected. Several authors, *e.g.* [13,37,38] among others, predict the appearance of at least one further feature besides the established single particle band and pair band (present below T^*, see [8]). Nevertheless, to exclude artifacts of the finite lattice calculations, we studied the evolution of the Ω_3-peak with system size. Figure 12 shows the size dependence of $\Omega_3(\pi,\pi)$ for lattice sizes N between 64 and 256 sites, for a $U/t = 6.0$, $\rho = 0.4$ system at temperature $T/t = 0.3$ (here we observed the strongest size dependency among all systems under investigation). Clearly, the position of the peak converges to a fixed value for $N \to \infty$. The peak itself becomes even more pronounced (*i.e.* its relative spectral weight allows an easy distinction from the rest of the structure), if we increase the system size. Figures 10 and 11 give the impression, that the pseudogap opens in this temperature regime and at $k \approx (\pi,\pi)$ between the Ω_2

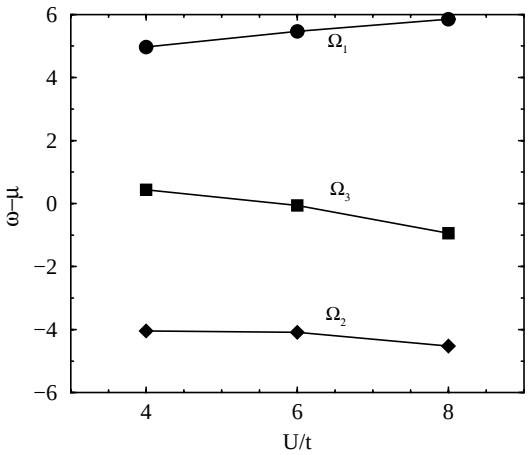

Fig. 11. Peak positions Ω_1, Ω_2 and Ω_3 as a function of coupling U, $k = (\pi, \pi)$, $\rho = 0.4$, $T/t = 0.5$.

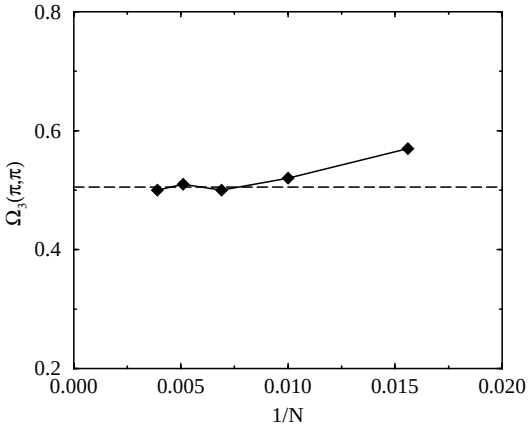

Fig. 12. Position of the central peak Ω_3 at $k = (\pi, \pi)$ in the band structure for $U/t = 6.0$, $\rho = 0.4$, $T = 0.3$ as a function of inverse system size $1/N = 1/L^2$ ($\diamond$); the dashed line indicates the supposed level for $L \to \infty$.

and Ω_3 peaks, not exactly at $\omega - \mu = 0$. This observation is at least qualitatively partially consistent with the work presented in [34]

4.3 Band structure

After having identified quite unconventional structures in $A(k, \omega)$ in Section 4.2 we want to discuss rather extended regions in k-space. For this purpose we plot $A(k, \omega)$ along the triangle $(0, 0) \to (\pi, 0) \to (\pi, \pi) \to (0, 0)$ in momentum space, which allows us an examination along the main lattice directions between zone center and corner. In principle, we would be interested in a "real band structure calculation" for the 2AHM, which would give us all bands and there dispersion. Using a special type of plot, we can extract some aspects of the bandstructure from the calculation of $A(k, \omega)$. We use a gray shade coding to plot the spectral function in the k-ω-plane, along the described k-path. The gray shades code the value of $A(k, \omega)$, a quartic folding form is used to get a non-linear coding (*i.e.* small values of $A(k, \omega)$ are strongly enhanced to visualize structures resulting from small peaks). Nevertheless, this type of plotting gives *not* the full band structure, since only branches with non-vanishing weight are visible. The reader should keep this in mind when comparing our data with "real" band structure calculations. As a starting point, Figure 13 depicts a band structure for the 2AHM, resulting from a simple BCS dispersion form $E^2(k) = \epsilon^2(k) + \Delta^2$, with a BCS gap Δ. This BCS band structure is shown for two different values of the chemical potential, one is close to the lower edge of the non-interacting band and the other one corresponds roughly to quarter-filling.

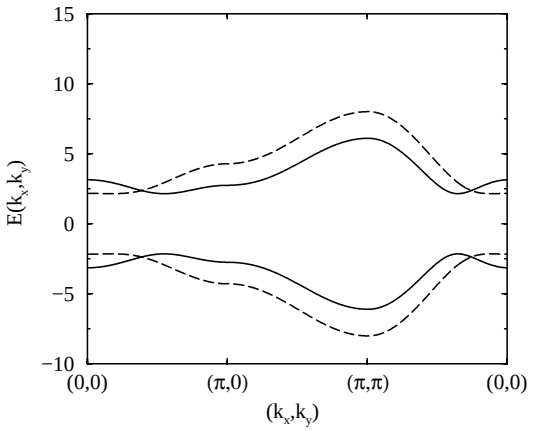

Fig. 13. Band structure resulting from a BCS calculation, $E^2(k) = \epsilon^2(k) + \Delta^2$. The dashed curve corresponds to a system where the chemical potential is close to the lower band edge of the non-interacting system (*i.e.* $\rho \to 0$), and the solid curve represents data, where μ is deep inside the noninteracting band.

In contrast, Figures 14–18 present QMC data. Figure 14 shows the band structure (the name is used in the following discussion as a synonym for the described gray coded $A(k, \omega)$ plot) for $U/t = 4.0$, quarter-filling $\rho = 0.25$ and a series of temperatures down to $T \approx T_c$. The $T/t = 2.0$ and $T/t = 0.11$ panels are the easiest ones to describe: $T/t = 2.0 \gg T^*$ and $T/t = 0.11 \approx T_c$. At a temperature $T \gg T^*$ we have only one band (which we denote, in accordance to Sect. 4.2, Ω_1), corresponding to the noninteracting system, pairs are thermally dissociated. Lowering the temperature ($T/t = 1.0$) causes the appearance of a second band, pairs start to form and occupy a pair band Ω_2 ("two-particle bound state") [8]. This second band is particularly pronounced at the zone center and zone corners. If we decrease the temperature further down to $T/t = 0.5$, we see a splitting of the Ω_2-band into two distinct branches in a region around the zone corner (π, π). This splitting starts for $T/t = 0.5$ at $k \approx (\pi, \pi/4)$, and the region expands (visible as some kind of "bubble" extending from (π, π)) if we go to lower temperatures $T/t = 0.3$, $T/t = 0.25$. For the last temperature we find three branches extending over the whole k-regime, besides the immediate neighborhood of the Fermi surface vector k_F. During this process, Ω_3 seems to shift towards higher frequencies. In the regime close to the transition region

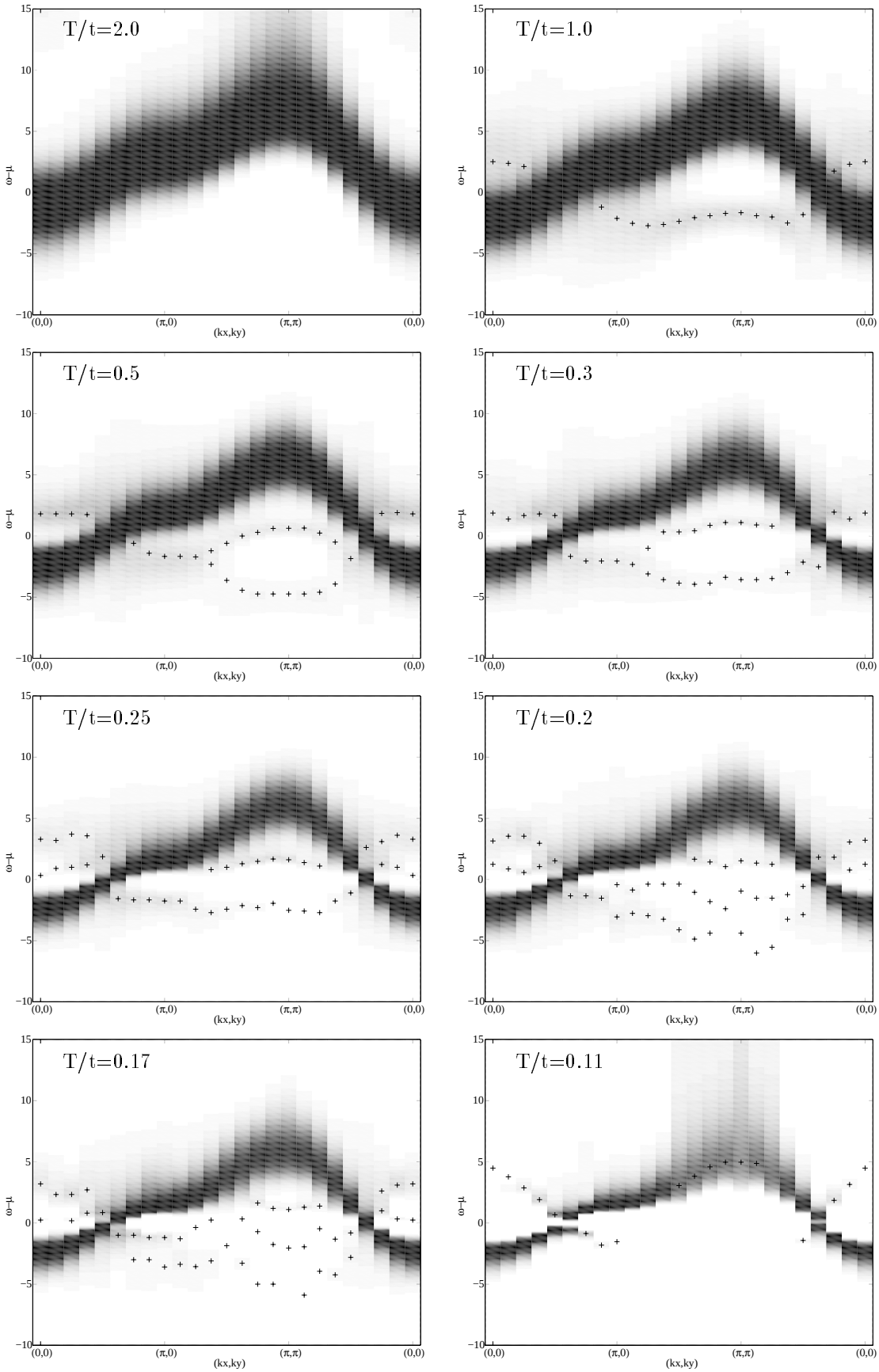

Fig. 14. QMC band structure, $U/t = 4.0$, $\rho = 0.25$. The crosses mark low peaks which otherwise are hardly visible in this plot.

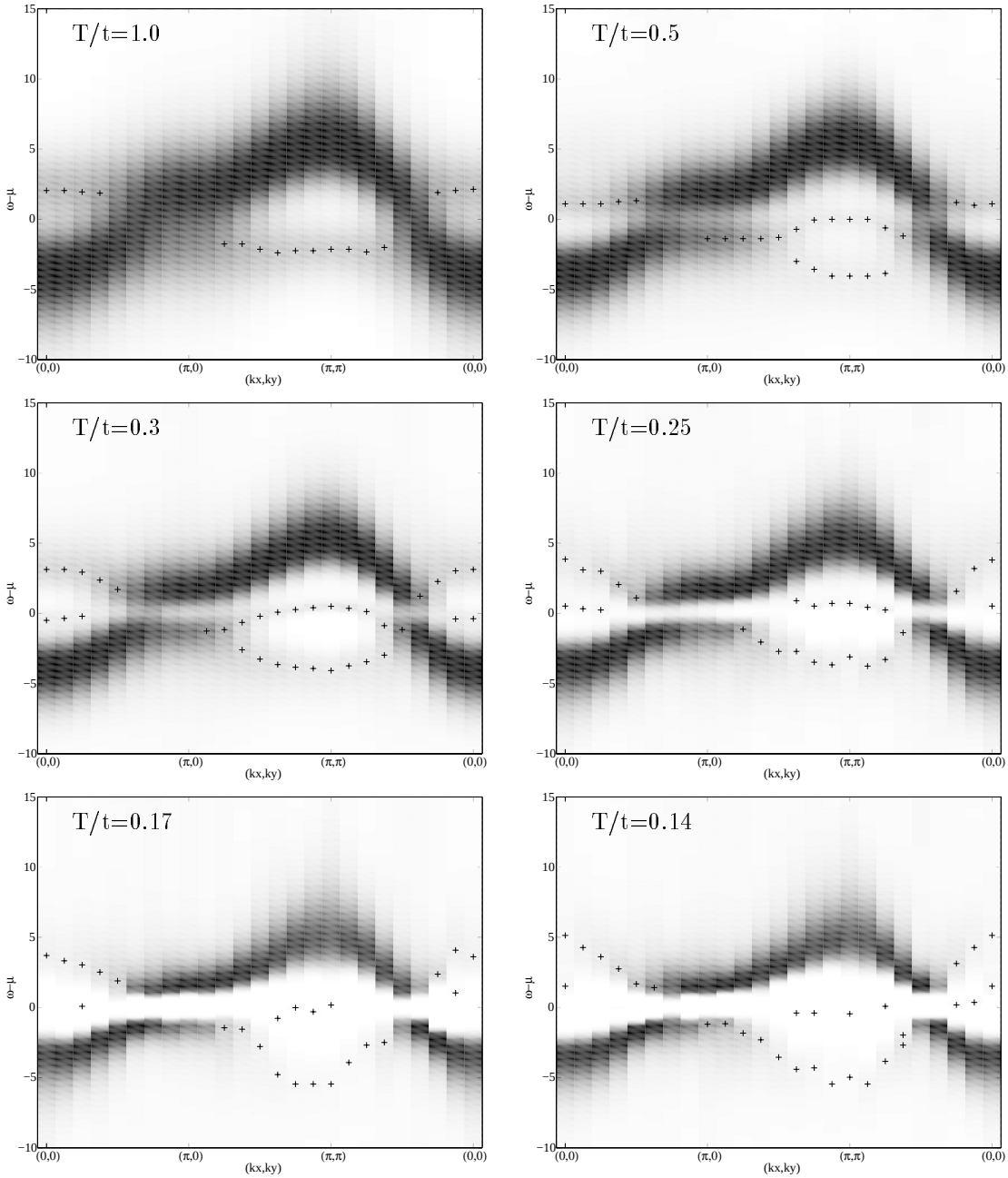

Fig. 15. QMC band structure, $U/t = 6.0$, $\rho = 0.4$.

around T_c we get another splitting, a fourth band evolves out of Ω_2, again initially around the zone corner. At T_c and below, the band structure becomes "conventional" again, the dispersion of the spectral weights is consistent with a band structure predicted for a usual (BCS-type) superconductor below T_c (compare with Fig. 13).

Similar data are provided for $\rho = 0.4$, $U/t = 6.0$ (Fig. 15) and $\rho = 0.1$, $U/t = 8.0$ (Fig. 16). The evolution of the band structure is similar, despite shifts of the particular bands due to the different filling and coupling strength values. Figure 16 is of particular interest, since the lower filling produces only weak many particle correlations in this "dilute" system, and it is possible to make at least qualitative comparisons to results from other methods, *e.g.* T-matrix calculations.

An interesting result obtained by Kagan *et al.* [13] is reproduced in Figure 17. There, we show their T-matrix band structure for a system with $\rho = 0.5$, $U/t = 10$ and $T/t = 0.1$ in the *normal* state (their [13] approach does not produce superconducting correlations, due to a explicit implementation of Mermin and Wagner's theorem [39]). The different branches are marked gray, if the particular spectral weight is close to zero, and thus would be invisible to our method. It is marked black, if the spectral weight is non-vanishing, so that we should be able to see the band. Unfortunately, [13] presents only data along

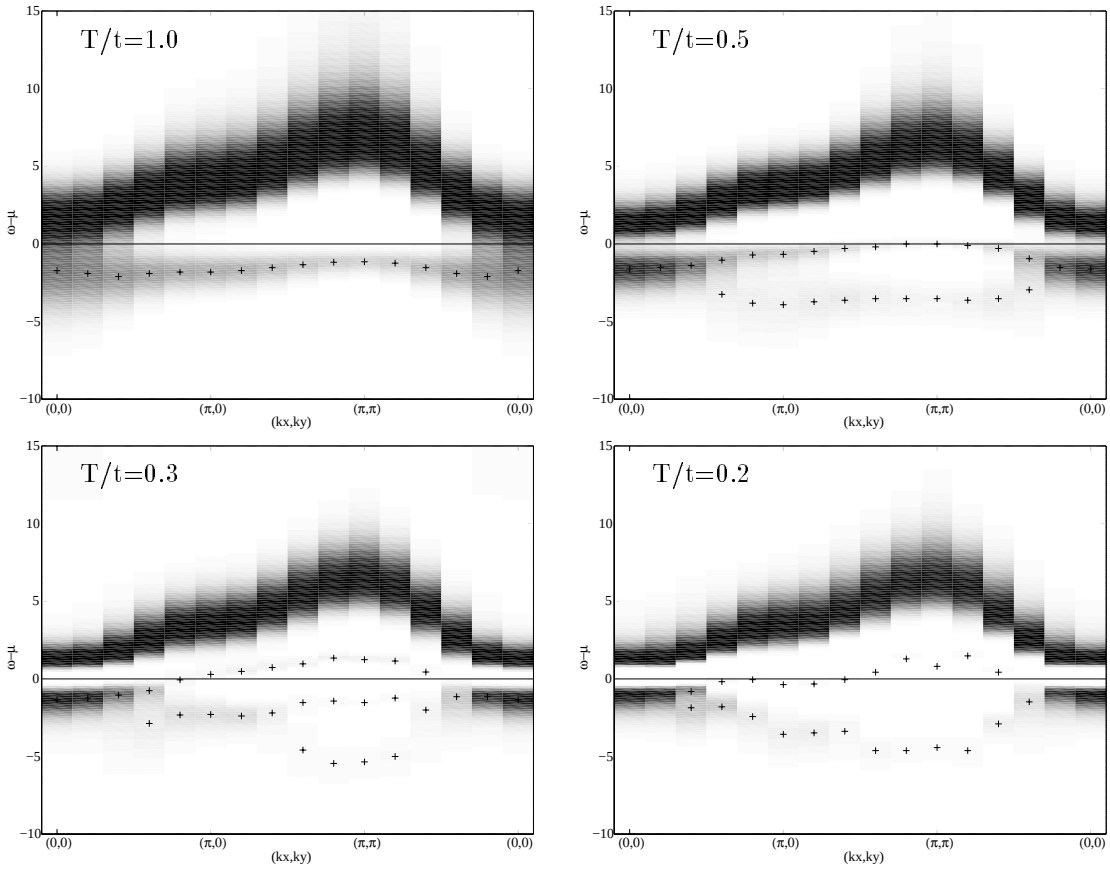

Fig. 16. QMC band structure, $U/t = 8.0$, $\rho = 0.1$.

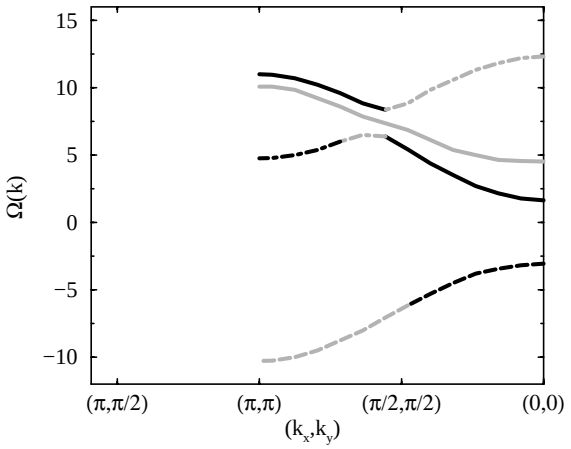

Fig. 17. Band structure $\Omega(k)$ from a T-matrix calculation, for $\rho = 0.05$, $U/t = 10$ and $T/t = 0.1$, data taken from [13]. The grey branches mark regions of the band structure with virtually zero spectral weight, thus, only the black parts would be "visible" in a plot using $A(k,\omega)$-data as shown in the presentation of the QMC "band structures".

the diagonal. Most important and interesting for a comparison to our data is the fact that these authors find a third branch resulting from the η resonance initially proposed by Yang [38], which – using our presentation technique – should be particularly pronounced around $k = (\pi, \pi)$. This mode has only a weak U-dependence. This branch comes down in energy with increasing U, similar to our results (see, *e.g.*, Fig. 11). It is necessary to compare the results of [13] with our QMC data taken at quite high temperatures, *e.g.* $T/t = 0.5$, since at lower temperatures, *e.g.* $T/t = 0.1$, the QMC system is dominated by superconducting correlations, as discussed before, causing additional changes in the band structure.

Finally, in Figure 18 we present a direct comparison between two bands for $U/t = 4$ and $U/t = 8$, both measured at $\rho = 0.4$ and $T/t = 0.5$. This figure shows the pronounced differences arising from the BCS to BEC crossover. In addition to the two coupling values presented in Figure 18 we ask the reader to consider also the uppermost right panel of Figure 15, $U/t = 6.0$, $\rho = 0.4$, $T/t = 0.5$, which can be regarded as an in-between panel for Figure 18. All three coupling values $U/t = 4.0$, $U/t = 6.0$ and $U/t = 8.0$ show two distinct bands in the normal state, but only $U/t = 8.0$ has a large, fully developed (pseudo-) gap around $\omega - \mu = 0$ for *all* k-vectors. In contrast, for $U/t = 4.0$ we find a single, ungapped peak at the k-vectors corresponding to the "Fermi"-surface (defined in the general sense as previously discussed). $U/t = 6.0$ marks somehow the crossover. Included in the right column of Figure 18 are also the corresponding k-space maps (there coding is described in detail in Sect. 4.4). Here, the effect of the crossover is even more easily seen: in contrast to the $U/t = 8$ case we find a clear "signature"

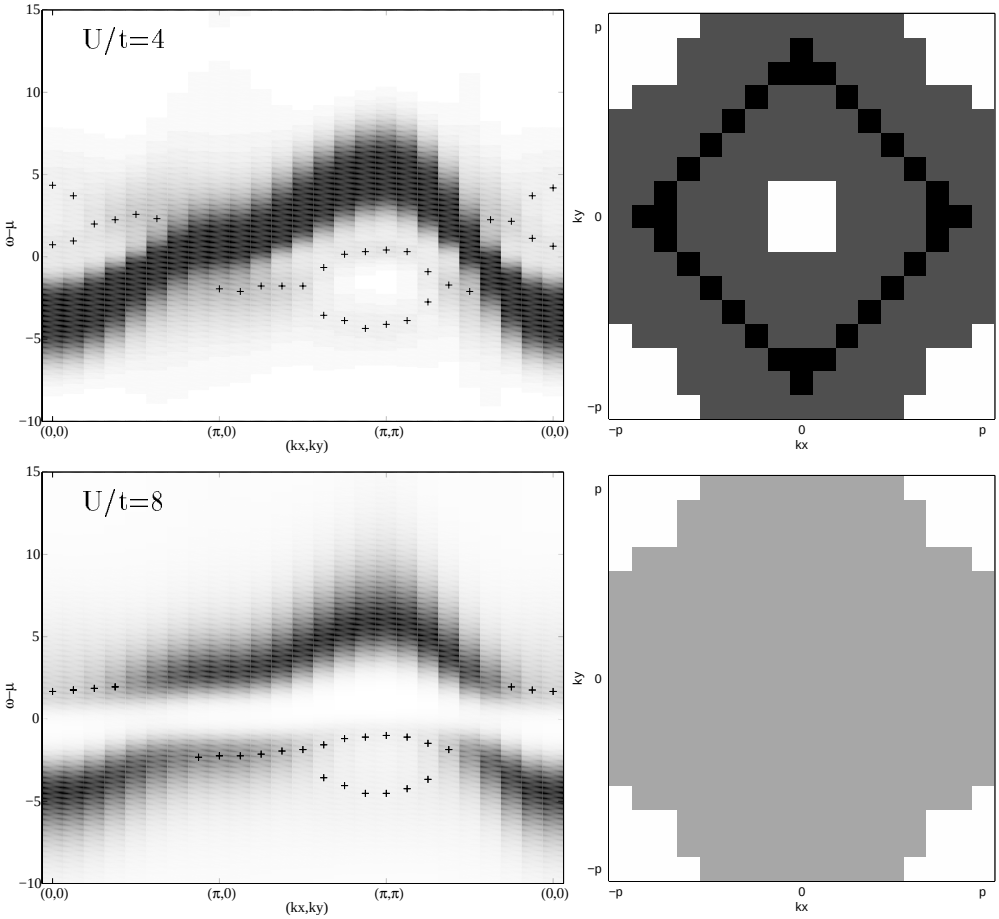

Fig. 18. QMC band structure (left column), $\rho = 0.4$, $T/t = 0.5$, $U/t = 4.0$ and $U/t = 8.0$, and affiliated k-space maps (right column).

of the "Fermi surface" (or rather its residues, signaled by the black pixels corresponding to ungapped k-points). Common to both cases is the "bubble" around (π, π), where the Ω_3-branch shows up, indicated by the white patches in the k-maps.

4.4 k-space maps

After the discussion of the spectral functions and the band structure we want to study systematically how certain features evolve in momentum space. For that purpose we use an unconventional approach: in Figure 19 we plot a particular type of map of the Brillouin zone $((-\pi, \pi), (-\pi, \pi))$. We use four different levels of gray shading to code the "type" of spectral density/band structure found at a particular k-point: a black square ("k-pixel") represents a k-point with a fully *ungapped* $A(k, \omega)$ (one peak), a dark gray k-pixel a *partially* developed gap (*i.e.* $A(k, 0) \neq 0$, but two distinct maxima), a light gray k-pixel a *fully* gapped spectral function, and a white k-pixel marks a k-point, which has a spectral function having *more than two* distinct peaks. Using this coding scheme we start with a totally "black" Brillouin zone for very high temperatures ($T/t = 2.0$), shown in the uppermost left corner of Figure 19. This patch is equivalent to the corresponding subpicture in Figure 14, and represents the fact that we have only one single band at this temperature, possible pairs are thermally dissociated.

On lowering the temperature, dark gray areas appear at the corners of the zone around (π, π) and equivalent points, signaling the opening of a "pseudo-gap" (*i.e.* a splitting of the single peak in $A(k, \omega)$ into two peaks). Further lowering of the temperature causes

(a) a growth of the gapped regions around (π, π);
(b) an additional "nucleus" of gapped states at the zone center around $(0, 0)$;
(c) finally a fully opened gap down to zero in this regions (uppermost row in Fig. 19). The temperature, where the initial opening of gapped k-regions is observed, will be called T^* in the further context of this paper. We would like to emphasize, that even in the case of a moderate coupling strength $U/t = 4$, this temperature T^* is about 15 times higher than T_c, the superconducting transition temperature. This is in contrast to the value presented in Section 4.1 as well as earlier publications, since a pure definition of T^* *via* the opening of a pseudogap in the density of states is rather less sensitive and gives a much lower temperature scale [10].

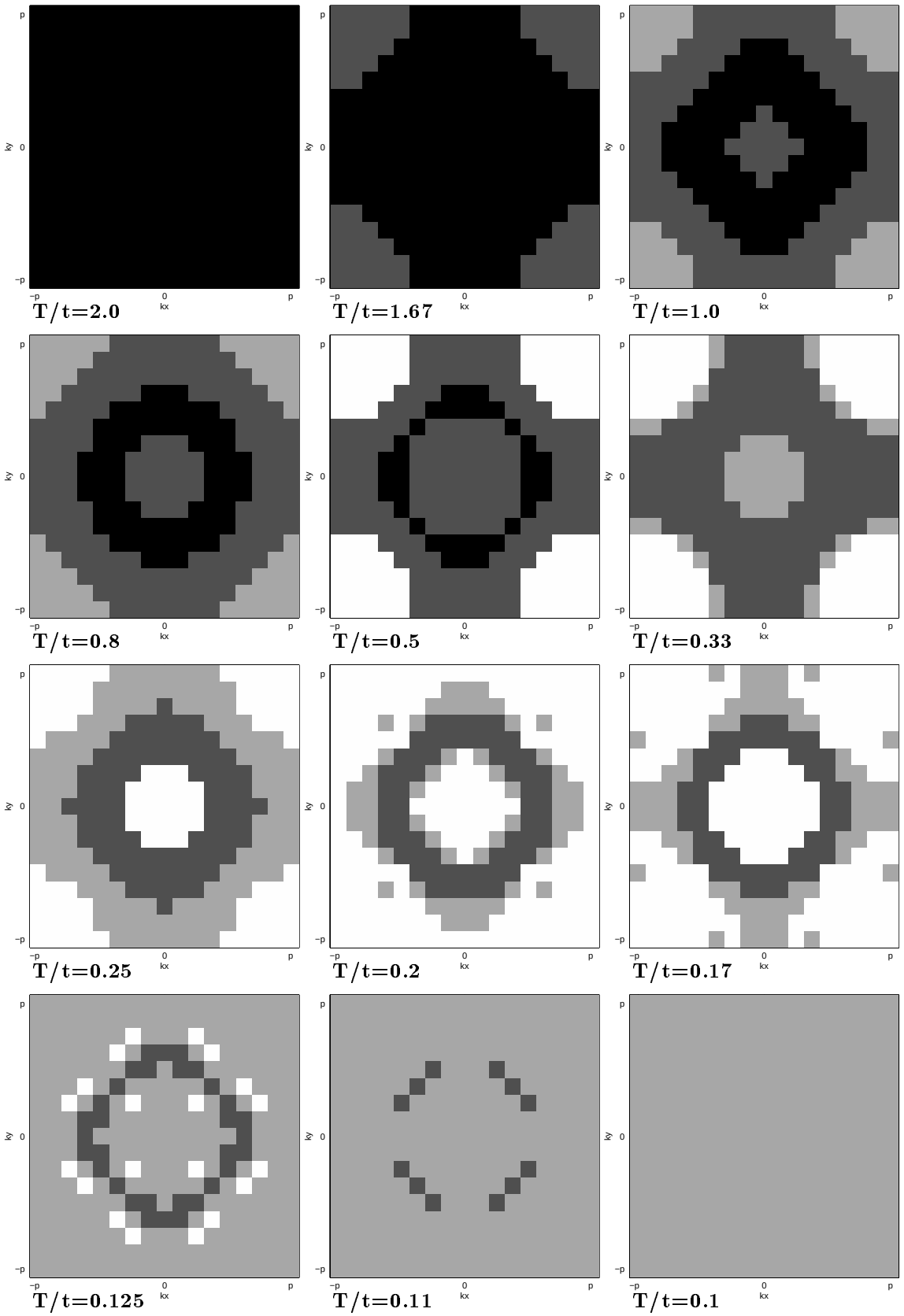

Fig. 19. k-space maps, $U/t = 4.0$, $\rho = 0.25$. Brillouin zone ($-\pi \leq k_{x,y} \leq \pi$) with each discrete k-point gray coded according to the "gap state" of it's $A(k, \omega)$. Coding scheme: *black* (ungapped), *dark gray* (two peaks, gap not fully developed down to zero), *light gray* (two peaks, fully developed gap) and *white* (more than two peaks).

Such an "accuracy dependency" is a typical feature of a smooth crossover in contrast to a phase transition. It should be stressed that the pseudogap obtained from an analysis of the DOS is directly connected to the pseudogap obtained from the static spin susceptibiltiy, *i.e.* the Knight shift [40], calculated for the same model and parameters.

If we lower the temperature further we approach a new regime in the k-maps, marked by the white k-pixels: we detect in the central map of the second row ($T/t = 0.5$) the appearance of k-points having three (and for even lower temperatures four) distinct maxima in the spectral function A. This patch again should be viewed together with the corresponding band structure, Figure 14. For temperatures $T/t > 0.5$ we had only two distinct branches, but now the lower one of the two bands starts to split up into two bands in a region around (π, π) and equivalent points (the "bubble" splitting Ω_2 corresponds to the white k-pixels in the k-maps). It seems important to note that this splitting starts in a similar k-region where the initial formation of a second band Ω_2 (*i.e.* the opening of the pseudo-gap) was observed.

Going to temperatures $T/t \leq 0.2$ we find that

(a) after an intermediate extension the white regimes finally disappear. The spectral weights on several of the peaks vanish, but not necessarily the bands itself;

(b) only a narrow "ring structure" of not fully gapped k-points remains, reflecting the exact position of the "Fermi surface" (defined rather in terms of a drop in the momentum distribution $n(k)$ than in a strict sense, as discussed earlier). This "ring structure" vanishes only close to and below $T_c = 0.11t$. Below T_c, a homogeneous patch is obtained. It is important to note that for this U-value the final opening of the gap *along* the Fermi surface happens only at T_c (+ a possible fluctuation window), resembling remnants of a BCS-type of transition (we again refer also to Fig. 8). In a conventional superconductor the so-called "Fermi-surface instability" at T_c is a characteristic feature of a BCS-type of theory. The fact that the gap along the Fermi surface seems to open at different temperatures for different directions is due to the finite lattice, which gives rise to only a finite number of k-points. Obviously, for the chosen filling $\rho = 0.25$ the Fermi surface lies in between of two k-points along the main axes, whereas it "hits" exactly along the diagonals.

Here we are really in a crossover regime, since we have a formation of a pseudogap, a second branch in the band structure and thus pairs at temperatures far above T_c, but a full opening of the gap along the Fermi surface takes place only at approximately T_c. This is particularly eminent in Figure 18, where we compare $U/t = 4$ and $U/t = 8$, both on the level of band structure and k-map plots (left and right columns, respectively). In the normal state system for $U/t = 4.0$ the "Fermi surface" is again clearly marked by the black k-pixels (similar to the $T/t = 0.5$-panel in Figure 14, but larger due to $\rho = 0.4$ in Figure 18 in contrast to $\rho = 0.25$, just as expected). In contrast, we have at the same temperature for $U/t = 8$ a fully gapped system. The extension of the white areas at the zone corners is identical, at the zone center we are not able to detect a splitting into more than two bands for $U/t = 8.0$ (and similarly for $U/t = 6.0$).

5 Discussion and conclusions

To summarize our results we have investigated the following problem.

We studied the 2AHM in the crossover regime between $U/t = 4$ and $U/t = 8$, which is – using Figure 1 as an illustration – just around the maximum of $T_c(U)$. A T_c-curve (or rather in a strict sense a T_{KT}-curve) can be obtained by *e.g.* QMC studies or even simpler using a combination of a BCS approach and a KT argumentation, as done by Denteneer *et al.* [41]. The latter gives a qualitatively correct picture (quantitatively it provides at least a reasonable upper bound), which allows an interpolation between the weak coupling BCS regime (with a monotonically increasing T_c) and the strong coupling BEC regime (with a monotonically decreasing T_c). Such a study of the phase diagram has been published *e.g.* in [10]. Here we want to go one step further and investigate the effects of this crossover on the density of states and band structure. First results have been published earlier, *e.g.* in [8] using QMC simulations, but also for example in [17] and other studies. Our presentation widely extends these previous data, and focuses in particular on the effects of the crossover on the density of states, the spectral densities and the band structure. We are able to show how remnants of the BCS concept (like a kind of "Fermi surface") "survive" into the crossover regime, whereas also precursors of the BEC (or better "preformed pair") regime appear quite early (like the second band). We notice that – although BCS theory is strictly valid only in the very limit of $U \to 0$ (and thus $T_c \to 0$) at the superconductor to normal conductor endpoint of the $T_c(U)$ phase line – remnants of a BCS/mean field type of transition are visible up to quite large values of U ($U/t \simeq 4$). Similarly interesting is the fact that the other endpoint of the phase transition line $T_c(U)$, the superconductor – insulator point at $U \to \infty$, has an even bigger bassin of attraction. It starts at $U/t \to \infty$ and goes down well below the maximum of the $T_c(U)$ curve into the BCS regime (taking the appearance of a second branch in the excitation spectrum as a marker). This confirms our earlier findings [42] analyzing an "Uemura"-type of plot for the 2AHM. The presented concepts have been studied over a wide parameter range, using simulations on rather large systems with a state-of-the-art QMC/MaxEnt simulation tool. It is difficult to decide on the origin of some of the observed effects (preformed, tightly bound pairs *versus* fluctuations or a combination) from the spectral properties only, but we will try to extend and supplement the presented data with measurements of other thermodynamic quantities as soon as possible. A really striking discovery is the appearance of more than two bands in a certain temperature regime $T^* > T > T_c$.

We would like to acknowledge interesting discussions with M.H. Pedersen, H. Beck, R. Frésard, M. Capezzali, R. Micnas, J. Engelbrecht and V. Loktev on the 2AHM and the crossover topic, P. Schwaller and J. Osterwalder on spectroscopy in "real" cuprates and H.-G. Matuttis on MaxEnt and QMC. This work was supported by the Swiss National Science Foundation.

References

1. See *e.g.*, J.R. Schrieffer, *Theory of Superconductivity* (Addison-Wesley, Reading, 1988).
2. See *e.g.*, J. Blatt, *Theory of Superconductivity* (Academic Press, New York, 1964); R. Micnas, J. Ranninger, S. Robaszkiewicz, Rev. Mod. Phys. **62**, 113 (1990).
3. H. Ding, T. Yokoya, J.C. Campuzano, T. Takahashi, M. Randeria, M.R. Norman, T. Mochiku, K. Kadowaki, J. Giapintzakis, Nature **382**, 51 (1996); H. Ding, J.C. Campuzano, M.R. Norman, M. Randeria, T. Yokoya, T. Takahashi, T. Takeuchi, T. Mochiku, K. Kadowaki, P. Guptasarma, D.G. Hinks, `cond-mat/9712100`.
4. A.G. Loeser, Z.-X. Shen, D.S. Dessau, D.S. Marshall, C.H. Park, P. Fournier, A. Kapitulnik, Science **273**, 325 (1996).
5. P. Schwaller, T. Greber, J.M. Singer, J. Osterwalder, P. Aebi, H. Berger, L. Forró (unpublished).
6. P. Coleman, Nature **392**, 134 (1998).
7. Ch. Renner, B. Revaz, K. Kadowaki, L. Maggio-Aprile, Ø. Fischer (unpublished); Ch. Renner, B. Revaz, J.-Y. Genoud, K. Kadowaki, Ø. Fischer, Phys. Rev. Lett. **80**, 149 (1998).
8. J.M. Singer, M.H. Pedersen, T. Schneider, H. Beck, H.-G. Matuttis, Phys. Rev. B **54**, 1286 (1996).
9. J.M. Singer, M.H. Pedersen, T. Schneider, Physica B **230-232**, 955 (1997).
10. J.M. Singer, T. Schneider, M.H. Pedersen, Eur. Phys. J. B **2**, 17 (1998).
11. Ph. Nozières, S. Schmitt-Rink, J. Low Temp. Phys. **59**, 95 (1985).
12. M. Drechsler, W. Zwerger, Ann. Phys. (Leipzig) **1**, 15 (1992).
13. M.Y. Kagan, R. Frésard, M. Capezzali, H. Beck, Phys. Rev. B **57**, 5995 (1998).
14. J.M. Kosterlitz, D.J. Thouless, J. Phys. C **6**, 1181 (1973).
15. A. Moreo, D.J. Scalapino, Phys. Rev. Lett. **66**, 946 (1991).
16. R. Micnas, T. Kostyrko, *Recent Developments in High Temperature Superconductivity*, edited by J. Klamut *et al.* (Springer, Berlin 1996).
17. R. Micnas, M.H. Pedersen, S. Schafroth, T. Schneider, J.J. Rodríguez-Núñez, H. Beck, Phys. Rev. B **52**, 16223 (1995).
18. M.H. Pedersen, J.J. Rodríguez-Núñez, H. Beck, T. Schneider, S. Schafroth, `cond-mat/9702173`.
19. T. Schneider, H. Beck, D. Bormann, T. Meintrup, S. Schafroth, A. Schmidt, Physica C **216**, 432 (1993).
20. O. Tchernyshyov, Phys. Rev. B **56**, 3372 (1997).
21. A.J. Leggett, J. Phys. IV France Colloque **41**, C7-19 (1980).
22. R. Haussmann, Z. Phys. B. **91**, 291 (1993); Phys. Rev. B **49**, 12975 (1994).
23. V. Loktev, S.G. Sharapov, Cond. Mat. Phys. **11**, 131 (1997); V.P. Gusynin, V.M. Loktev, S.G. Sharapov, `cond-mat/9709034`; V.M. Loktev, V.M. Turkowski, `cond-mat/9707191`.
24. M. Randeria, *Bose-Einstein Condensation*, edited by A. Griffin *et al.* (Cambridge University Press, Cambridge, England, 1994); M. Randeria, *Proc. Adriatico Res. Conf.*, *Fluctuation Phenomena in High Temperature Superconductors*, edited by M. Ausloos *et al.* (Kluwer Academic, The Netherlands, 1996); M. Randeria *et al.*, Phys. Rev. Lett. **41**, 327 (1990).
25. N. Trivedi, M. Randeria, Phys. Rev. Lett. **75**, 312 (1995); M. Randeria, N. Trivedi, A. Moreo, R. Scalettar, Phys. Rev. Lett. **69**, 2001 (1992).
26. J.E. Hirsch, Phys. Rev. B **31**, 4403 (1985);
27. H.-G. Matuttis, Ph.D. thesis, University of Regensburg, Germany, 1995.
28. E.Y. Loh Jr., J.E. Gubernatis, R.T. Scalettar, R.L. Sugar, S.R. White, *Proc. Workshop on Interacting Electrons in Reduced Dimensions*, edited by D. Baeriswyl, D.K. Campbell (Plenum Press, New York, 1989).
29. M. Ulmke, H. Müller-Krumbhaar, Z. Phys. B **86**, 383 (1992).
30. W. von der Linden, Phys. Rep. **220**, 53 (1992).
31. M. Jarrell, J.E. Gubernatis, Phys. Rep. **269**, 133 (1996).
32. R.N. Silver, D.S. Sivia, J.E. Gubernatis, M. Jarrell, Phys. Rev. Lett. **65**, 496 (1990); J. Gubernatis, M. Jarrell, R.N. Silver, D.S. Sivia, Phys. Rev. B **44**, 6011 (1991); R.N. Silver, D.S. Sivia, J.E. Gubernatis, Phys. Rev. B **41**, 2380 (1990); R.N. Silver, D.S. Sivia, J.E. Gubernatis, *Quantum Simulations of Condensed Matter Phenomena*, edited by J.E. Gubernatis, J.D. Doll (World Scientific, Singapore, 1990).
33. J.R. Engelbrecht, A. Nazarenko, `cond-mat/9806223`.
34. M. Letz, R.J. Gooding, `cond-mat/9802107`.
35. A. Schmid, Z. Phys. **231**, 324 (1970).
36. E. Abrahams, M. Redi, C. Woo, Phys. Rev. B **1**, 280 (1970).
37. A.I. Solomon, K.A. Penson, `cond-mat/9712228`.
38. C.N. Yang, Phys. Rev. Lett. **63**, 2144 (1989).
39. N.D. Mermin, H. Wagner, Phys. Rev. Lett. **17**, 1133 (1966); P.C. Hohenberg, Phys. Rev. **158**, 383 (1967).
40. J.M. Singer, P.F. Meier, Physica C (to appear, 1998).
41. P.J.H. Denteneer, Guozhong An, J.M.J. van Leeuwen, Phys. Rev. B **47**, 6256 (1993); P.J.H. Denteneer, Guozhong An, J.M.J. van Leeuwen, Europhys. Lett. **16**, 5 (1991).
42. T. Schneider, J.M. Singer, Europhys. Lett. **40**, 79 (1997).